2D Vibrational Exciton Nanoimaging of Domain Formation in Self-Assembled Monolayers

Thomas P. Gray, Jun Nishida, Samuel C. Johnson, and Markus B. Raschke*

ACCESS | Metrics & More | Article Recommendations | SI Supporting Information

ABSTRACT: Order, disorder, and domains affect many of the functional properties in self-assembled monolayers (SAMs). However, carrier transport, wettability, and chemical reactivity are often associated with collective effects, where conventional imaging techniques have limited sensitivity to the underlying intermolecular coupling. Here we demonstrate vibrational excitons as a molecular ruler of intermolecular wave function delocalization and nanodomain size in SAMs. In the model system of a 4-nitrothiophenol (4-NTP) SAM on gold, we resolve coupling-induced peak shifts of the nitro symmetric stretch mode with full spatio-spectral infrared scattering scanning near-field optical microscopy. From modeling of the underlying 2D Hamiltonian, we infer domain sizes and their distribution ranging from 3 to 12 nm across a field of view on the micrometer scale. This approach of vibrational exciton nanoimaging is generally applicable to study structural phases and domains in SAMs and other molecular interfaces.

KEYWORDS: vibrational exciton, infrared spectroscopy, scattering scanning near-field optical microscopy (s-SNOM), molecular vibrations, self-assembled monolayers, tip-enhanced Raman spectroscopy (TERS)
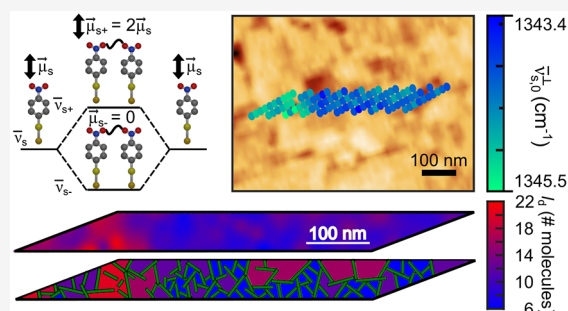
Self-assembled monolayers (SAMs) control the surface functionalities of a wide range of materials with applications including nanolithography,[1] molecular electronics,[2] protein biosensors,[3] and photocatalysis.[4] However, multiscale disorder, from point defects to domain formation, can disrupt the desired interfacial characteristics.[5] While conventional techniques such as optical ellipsometry and angle-resolved X-ray photoelectron spectroscopy (ARXPS) offer macroscopic average sample properties, they provide limited insight into the heterogeneity of the sample.[6] Conversely, while scanning tunneling microscopy (STM) offers high spatial resolution to directly observe defects and domains, it is not sensitive to cooperative effects between molecules.

Nevertheless, intermolecular coupling and collective effects between surface molecules often control the fundamental properties of SAMs. Measurement of that coupling can thus serve as a sensitive probe of local disorder. The coupling manifests itself in electronic or vibrational wave function delocalization that gives rise to hybridization with vibrational mode splitting and resonance energy shifts as spectroscopic observables. In particular, vibrational excitons, delocalized across domains in dense, well-ordered molecular systems, are sensitive to disorder and domain size.[7,8] However, with dimensions typically on the few-nanometer scale for many alkanethiol and aromatic thiol SAMs,[9,10] probing disorder in SAMs with the desired simultaneous high spatial resolution,

monolayer sensitivity, and spectroscopic specificity has long remained difficult.

In this Letter, we demonstrate vibrational exciton nanoimaging using infrared (IR) vibrational scattering scanning near-field optical microscopy (s-SNOM) as a local probe of molecular disorder and domain size in SAMs (Figure 1A). IR s-SNOM offers a field of view that spans micrometers while being sensitive to heterogeneity across many domains as well as intermolecular dipole coupling within domains. We studied the SAM of 4-nitrothiophenol (4-NTP) as a model system because of its relevance in photochemical reactions.[4,11,12] It is characterized by a distribution of lying-down and standing-up phases characteristic of short-chain alkanethiols[13] and thiophenols,[10] as shown in Figure 1B,C. We accomplish domain size imaging by first evaluating the vibrational coupling of the NO_2 symmetric stretch in 4-NTP SAMs with controlled density of the vibrational probe through dilution with thiophenol. We then model the SAM via a 2D interaction Hamiltonian to derive the delocalization lengths of local vibrational excitons, which we relate to the domain size. While
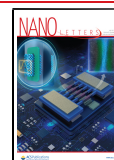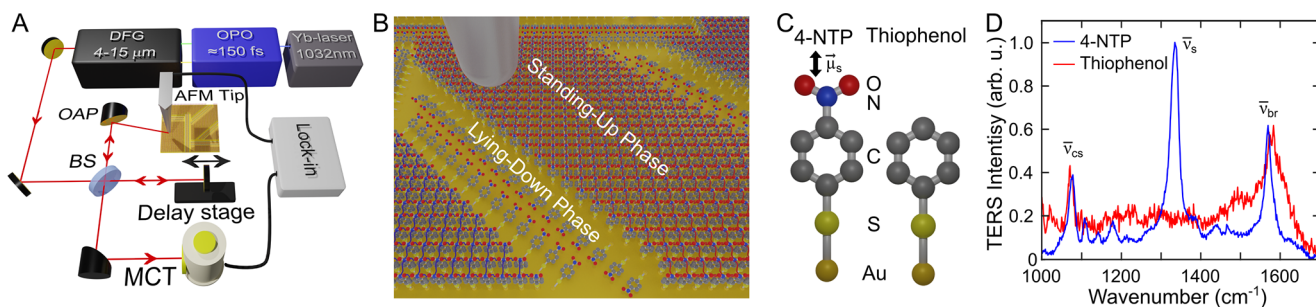
Figure 1. (A) Schematic of nano-FTIR *s*-SNOM. (B) Representation of domain formation in 4-NTP monolayers on Au(111). (C) Molecular structures of 4-NTP and thiophenol with the transition dipole moment of the nitro symmetric stretch mode labeled. (D) TERS of 4-NTP (blue) and thiophenol (red) spectra with $\overline{\nu}_{cs} = 1082$ cm^{-1}, $\overline{\nu}_s = 1337$ cm^{-1}, and $\overline{\nu}_{br} = 1577$ cm^{-1} peaks labeled.
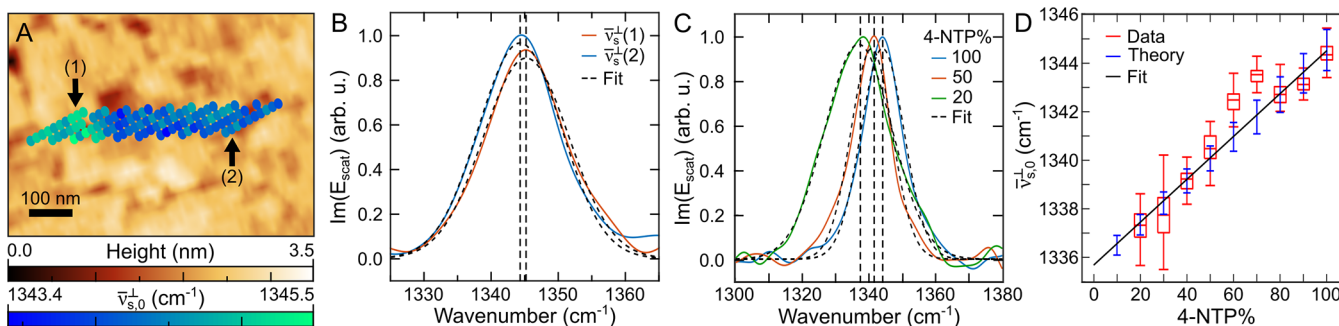
Figure 2. (A) Nanoscale map of spectral variation in $\overline{\nu}_{s,0}^{\perp}$ in a 100% 4-NTP monolayer with 15 nm spatial resolution. (B) Representative spectra and fits (black) of $\overline{\nu}_s^{\perp}$ at locations indicated in (A) with $\overline{\nu}_{s,0}^{\perp} = 1344.3 \pm 0.2$ cm^{-1} (blue) and 1345.2 ± 0.2 cm^{-1} (red) respectfully. (C) Representative spectra and fits (black) of 100% (blue), 50% (red), and 20% (green) 4-NTP monolayers. (D) Distribution of experimentally measured $\overline{\nu}_{s,0}^{\perp}$ (red) for mixed SAMs with different ratios, with theoretical values from vibrational exciton modeling (blue) and the fit of the experimental values (black).

real-space imaging of domain size is beyond the nominal spatial resolution limit of *s*-SNOM, we indirectly infer the domain sizes ranging from 3 to 12 nm across a field of view representative of the whole sample.

4-NTP (Figure 1C, left) (Sigma-Aldrich, lot no. MKCC1440, 90%) and thiophenol (Figure 1C, right) (Sigma-Aldrich, lot no. SHBK7577, 99.9%) were used without further purification to prepare SAMs on template-stripped gold.[6] Mixed SAMs were prepared using ethanol solutions of 4-NTP and thiophenol in molar ratios varying from 9:1 (90% 4-NTP) to 1:9 (10% 4-NTP).[14] Samples of 100% 4-NTP (Figure 1D, blue) and 100% thiophenol (Figure 1D, red) were then precharacterized by tip-enhanced Raman spectroscopy (TERS) (modified OmegaScope-R, Horiba Scientific). The C–S stretch mode ($\overline{\nu}_{cs} = 1082$ cm^{-1}) and phenyl ring mode ($\overline{\nu}_{br} = 1577$ cm^{-1}) are present in both spectra, while the strong N–O stretch mode ($\overline{\nu}_s = 1337$ cm^{-1}) is present only in the 4-NTP monolayer, as expected.[15−17]

We then performed broadband femtosecond IR *s*-SNOM with high sensitivity and spectral precision (customized nanoIR2-s prototype, Anasys Instruments/Bruker; see the Supporting Information for details) (Figure 1A).[8,18] We used $\overline{\nu}_s$ as a marker resonance of both pure 4-NTP and mixed monolayers. As established previously,[19−22] we performed vector near-field nanoimaging based on the anisotropic out-of-plane field enhancement from the optical antenna tip to selectively probe the out-of-plane component $\vec{\mu}_s^{\perp}$ of the N–O stretch ($\overline{\nu}_s^{\perp}$) and thus the standing-up domains of 4-NTP. Conversely, for the lying-down phase, $\vec{\mu}_s^{\parallel}$ is perpendicular to the tip axis and therefore provides a negligible signal contribution. From spatio-spectral analysis of the line shape

variations in $\overline{\nu}_s^{\perp}$, we then inferred the spatial delocalization of the intermolecular wave function, as illustrated in Figure 1B.

Figure 2A shows the spatial variation in the peak position of $\overline{\nu}_s^{\perp}$ as determined by Gaussian fitting of each spectrum. With ~15 nm spatial resolution, spectral shifts of up to 2 cm^{-1} can be seen across the surface with no correlation to topography (Figure S1), where $\overline{\nu}_{s,0}^{\perp}$ ranges from 1343.4 ± 0.2 cm^{-1} to 1345.5 ± 0.2 cm^{-1} (representative spectra are shown in Figure 2B). The corresponding full width at half-maximum (fwhm) varies from $\Gamma(\overline{\nu}_s^{\perp}) = 13$ cm^{-1} to $\Gamma(\overline{\nu}_s^{\perp}) = 17$ cm^{-1} without a noticeable spatial trend.

We then acquired spatio-spectral *s*-SNOM images of the mixed SAMs (representative data are shown in Figure S2). At densities as low as 5% 4-NTP, corresponding to ~100 IR-active oscillators,[10,23] the spectral peak was still discernible. However, below 20% 4-NTP, accurate fitting of $\overline{\nu}_{s,0}^{\perp}$ was not possible because the signal-to-noise ratio was too low. Representative spectra for 100%, 50%, and 20% 4-NTP are shown in Figure 2C, and the range of $\overline{\nu}_{s,0}^{\perp}$ fit values for different concentrations are presented in Figure 2D (red). Overall, a red shift of ~7 cm^{-1} with decreasing 4-NTP concentration is observed, starting from $\overline{\nu}_{s,0}^{\perp} = 1344.5 \pm 1.0$ cm^{-1} for 100% 4-NTP to $\overline{\nu}_{s,0}^{\perp} = 1337.3 \pm 1.0$ cm^{-1} for 20% 4-NTP. This spectral red shift can be attributed to weaker vibrational coupling due to an increase in the average nitro group separation.[24] A linear fit (Figure 2D, black) to the experimental fit values (red) provides an extrapolated uncoupled nitro resonance frequency of $\overline{\nu}_{s,0}^{\perp} = 1335.7$ cm^{-1}, representative of the nitro group of isolated 4-NTP molecules. The red shift is correlated with a spectral broadening from $\Gamma(\overline{\nu}_s^{\perp}) = 15 \pm 2$ cm^{-1} for 100% 4-NTP SAMs to $\Gamma(\overline{\nu}_s^{\perp}) = 23 \pm 3$ cm^{-1} for 20% 4-NTP SAMs. As

discussed below, this is expected on the basis of inhomogeneous broadening at lower concentrations.

We attribute the spatial heterogeneity observed in $\bar{\nu}_{s,0}^{\perp}$ to a spatially varying degree of intermolecular coupling resulting from domains of 4-NTP molecules with different orientations, as discussed below. Previous STM studies showed that 4-NTP SAMs form distinct nanoscale domains of molecules in both lying-down and standing-up configurations, with each occupying ∼50% of the surface,[10] as shown schematically in Figure 1B. The standing-up phase clumps in stripelike areas with anisotropic dimensions ranging from 2.5 to 6 nm in one direction and 2.5 to 15 nm in the other.

We modeled the observed spectral shifts in terms of the number of coupled molecules, which we used to determine the standing-up domain size. To describe the continuous red shift in $\bar{\nu}_{s,0}^{\perp}$ with the dilution of interacting nitro groups, we treated the vibrational wave function delocalization of neighboring nitro groups in the standing-up phase as vibrational excitons.[8,25,26] Vibrational excitons form through transition dipole coupling under conditions of tight packing or large transition dipole moments (TDM). The dipole coupling energy term $\hat{V}_{nm}$ for any two molecules m and n is given by

$$\hat{V}_{mn} = \frac{1}{4\pi\epsilon_0 |\vec{r}|^3}\left[\vec{\mu}_m\cdot\vec{\mu}_n - \frac{3(\vec{\mu}_m\cdot\vec{r})(\vec{\mu}_n\cdot\vec{r})}{|\vec{r}|^2}\right] \quad (1)$$

where $\vec{\mu}_m$ and $\vec{\mu}_n$ are the corresponding TDM values and $\vec{r}$ is their intermolecular spacing. For $\hat{V}_{mn} \ll \bar{\nu}_0$, the new eigenstates can be calculated from first-order perturbation theory within the tight binding model. In the case of two standing-up 4-NTP molecules with a typical intermolecular separation of 0.37 nm in a dense monolayer[23] and a TDM value of $|\vec{\mu}_{4NTP}| = 0.127$ D, the value $\hat{V}_{mn} = 1.6$ cm^{-1} is obtained, leading to splitting of $\bar{\nu}_s^{\perp}$ into two modes $\bar{\nu}_{s-}^{\perp}$ and $\bar{\nu}_{s+}^{\perp}$ with an energy splitting of $\Delta\bar{\nu}_s^{\perp} = 2\hat{V}_{mn} = 3.2$ cm^{-1}, as shown in Figure 3A. The $\bar{\nu}_{s+}^{\perp}$ mode, where the neighboring nitro groups oscillate in phase with respect to each other, has an out-of-plane TDM of $\vec{\mu}_{s+}^{\perp} = 2\vec{\mu}_s$ and thus is

IR-active. In contrast, the out-of-phase stretch mode $\bar{\nu}_{s-}^{\perp}$ with $\vec{\mu}_{s-}^{\perp} = 0$ is IR-inactive. While the interaction between two molecules leads to a red shift of only 1.6 cm^{-1}, i.e., an order of magnitude less than the observed ∼10 cm^{-1} red shift, in a 2D ensemble, the 4-NTP molecules form a vibrational superposition state within a standing-up domain, leading to a much larger shift. In contrast, the coupling between domains with orthogonally oriented 4-NTP molecules is negligible, and the lying-down molecules remain uncoupled.

To show the vibrational exciton formation on a 2D grid, we first modeled 4-NTP as a rectangular unit cell with standing-up domains ranging from 1 to 50 molecules on a side and lattice constants of $a = 0.43$ nm and $b = 0.37$ nm from known packing densities.[23] To match the experimental data in Figure 2D, the extrapolated uncoupled nitro resonance frequency $\bar{\nu}_{s,0}^{\perp} = 1335.7$ cm^{-1} was used for the ground-state energy. Additionally, $|\vec{\mu}_{4NTP}| = 0.127$ D was used to match the observed change in $\bar{\nu}_{s,0}^{\perp}$ with dilution. For each domain size (l_d), all of the off-diagonal coupling terms of the Hamiltonian were then calculated, and the Hamiltonian was diagonalized to solve for the corresponding eigenvalues and eigenvectors. The eigenvectors describe the relative TDMs for the individual molecules in the grid for a given quantum state and can be summed to find the total TDM of each coupled state, defining the relative IR activity of each coupled state. A weighted average across all states, $[\sum_i |\vec{\mu}_i|^2\bar{\nu}_i]/\sum_i |\vec{\mu}_i|^2$, then gives the $\bar{\nu}_{s,0}^{\perp}$ value for the initial 2D grid. For a 100% 4-NTP lattice, ≥90% of the relative IR activity is in a single eigenstate. As can be seen in Figure 3B (blue), a pronounced blue shift of 7 cm^{-1} in $\bar{\nu}_{s,0}^{\perp}$ occurs as l_d increases from 1 to 6 molecules. This is followed by a more gradual blue shift of 2 cm^{-1} from 1343.2 to 1345.5 cm^{-1} as l_d is increased from 7 to 22 molecules, which is only slightly larger than the observed experimental shift of 1343.4 cm^{-1} to 1345.5 cm^{-1} (black dashed). $\bar{\nu}_{s,0}^{\perp}$ continues to blue-shift at larger domain sizes but is outside the range of observed values.

In the case of mixed SAMs of 4-NTP and thiophenol, the resulting eigenvectors and eigenstates are sensitive to the spatial distribution of nitro groups. To account for this effect, 1000 grids were simulated with different random distributions. The effect of the dilution of nitro groups for mixed monolayers on the dependence of $\bar{\nu}_{s,0}^{\perp}$ on l_d in the cases of 60% 4-NTP monolayers (red) and 20% 4-NTP monolayers (green) is shown in Figure 3B. To a good approximation, the blue shift is linearly correlated with the degree of dilution. Additionally, there is a significant broadening of ±0.5 cm^{-1} in the $\bar{\nu}_{s,0}^{\perp}$ distribution for each domain size in both the 60% and 20% 4-NTP models due to the random nature of the dilution. In addition to broadening the $\bar{\nu}_{s,0}^{\perp}$ distribution between simulations, within a single simulation a broader range of local chemical environments distributes the IR activity across a wider range of eigenstates in mixed SAMs than in the 100% 4-NTP case. This inhomogeneous broadening leads to a spectral broadening as observed experimentally. To model the expected vibrational frequencies of standing-up domains of 4-NTP as observed in STM,[10] we simulated 1000 2D rectangular grids of molecules with random side lengths of 3−6 nm for the short axis and 3−15 nm for the long axis[10] for each mixed monolayer studied in Figure 2D (red). The 95% bounds of $\bar{\nu}_{s,0}^{\perp}$ versus concentration are shown in Figure 2D (blue) for comparison to the experimental values. The good agreement of the modeled vibrational exciton blue shift as a function of dilution
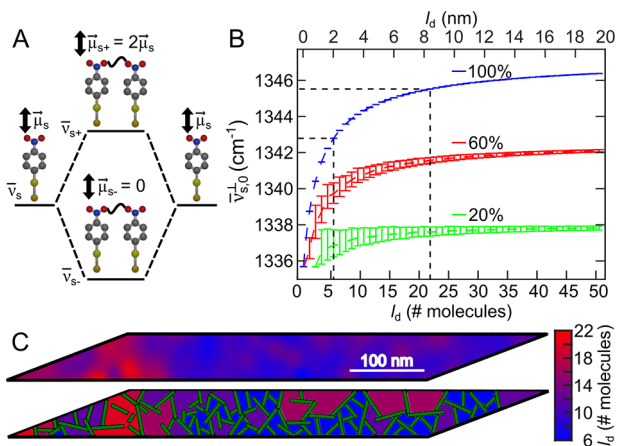
Figure 3. (A) Energy level diagram for transition dipole coupling between two neighboring molecules in a standing-up domain. (B) Modeled blue shift of $\bar{\nu}_{s,0}^{\perp}$ with increasing domain size for a 100% 4-NTP monolayer (blue), 60% (red), and 20% (green) mixed monolayers. (C) Top panel: Domain size of nanoimaging from Figure 2A as determined by (B). The range of l_d observed experimentally in 100% 4-NTP SAMs is indicated in (B) with black dashed lines. Bottom panel: schematic of the associated domain size distribution (with the lying-down phase shown in green).

with the experimental results (red) supports the validity of the model and underlying domain size distribution.

We next used the relationship between $\overline{\nu}_{s,0}^{\perp}$ and l_d as established from the model as a lookup table (Figure 3B, blue) and applied it to the spectral map of $\overline{\nu}_{s,0}^{\perp}$ from Figure 2A to derive the underlying spatial variation of l_d and thus the domain size. The resulting image (Figure 3C, top) shows l_d varying from 22 molecules (8.8 nm) on its left side to 7 molecules (2.8 nm) on its right side, corresponding to the short axis of standing-up 4-NTP domains of 2.5–6.0 nm from STM.[10] The model and interpretation are based on the assumption of pure 4-NTP and thiophenol monolayers. Thiolated impurities in the 4-NTP might lead to at most a 10% error in the surface nitro group concentration. The worst case of only 90% purity in a supposed 100% 4-NTP monolayer would broaden the distribution of $\overline{\nu}_{s,0}^{\perp}$ for a given domain size by less than ±0.1 cm^{-1}, which is much smaller than the observed 2 cm^{-1} shifts. Furthermore, surface roughness would disrupt the molecular order and weaken the intermolecular coupling. To illustrate the sensitivity of vibrational excitons to the local chemical environment, we estimated monatomic gold steps to cause a red shift of <0.3 cm^{-1} by raising half of our molecular grid by 0.24 nm.[27] This small red shift would also have only a negligible effect on the resolution of the model. For more complex molecular systems, higher-order effects such as modeling beyond point transition dipoles and inhomogeneous broadening of $\overline{\nu}_0$ might need to be considered. Such effects can lead to an asymmetric molecular response that requires full spectral line shape reconstruction for resonance fitting as opposed to our Gaussian fits.[28]

Conceptually, our measurements and modeling demonstrate vibrational exciton nanoimaging to spatially resolve sample characteristics down to the molecular scale, i.e., smaller than the nominal spatial resolution of IR s-SNOM. Here the vibrational exciton effectively serves as a quantum sensor through its vibrational wave function delocalization to sensitively probe molecular disorder and domain size. Mapping $\overline{\nu}_{s,0}^{\perp}$ to l_d is possible with domain sizes of up to tens of nanometers as long as $d\overline{\nu}_{s,0}^{\perp}(l_d)/dl_d$ can be discerned experimentally. For long-range order, $d\overline{\nu}_{s,0}^{\perp}(l_d)/dl_d$ would converge to 0, and the associated large domain size would become unsolvable yet also become directly accessible within the spatial resolution of s-SNOM.

We previously used this method to map domain sizes in 3D molecular crystals[8] without a structured benchmark for the independent validation of the model. In 4-NTP we now are able to compare the spectral scale of vibrational exciton delocalization derived from the model with structural information from STM studies,[10] validating both the method and previous results.

This method of vibrational exciton nanoimaging is beneficial in molecular systems where the domain size and intermolecular interactions affect functional properties such as carrier mobility and transport. Domain size and molecular order in SAMs affect the carrier mobility in SAM-based organic thin-film transistors.[29] Additionally, with slightly higher spectral resolution beyond 0.1 cm^{-1}, it may even become possible to detect and count pinhole defects in monolayers with long-range order, which diminish the performance of, e.g., superhydrophobic surfaces and organic electronics.[5]

As the modeled domains grow beyond tens of nanometers, $\overline{\nu}_0$ asymptotically approaches a constant value and becomes insensitive to the domain size. However, it remains sensitive to

effects such as disorder and defect density, which can then be measured. As the domains grow larger than the size of the tip, the measured molecules remain coupled to the entire domain and report a state larger than the tip resolution itself (nonlocal optical response). This would lead to a homogeneous s-SNOM response within the domain, which could be an interesting direction for future experiments. However, beyond transition dipole coupling, other effects such as coupling through phonons and the formation of phonon-bound states could dominate the vibrational landscape, as in hydrogen-terminated silicon surfaces.[30]

In summary, we used vibrational excitons in 4-NTP monolayers as a sensitive probe to image domain sizes using IR s-SNOM. This was accomplished by first quantifying the strength of intermolecular coupling through dilution of the monolayer with thiophenol. Probing at a sensitivity as low as ∼10^2 molecular oscillators, we found that the average delocalization length varies between 7 and 22 molecules (2.8 to 8.8 nm), reflecting the domain sizes of the standing-up phases.

Because of the sensitivity of vibrational excitons to molecular packing and orientation, this method is generally applicable to other molecular systems with strong mid-infrared vibrational transitions or a high density of oscillators and short-range order. Beyond characterizing delocalization lengths and defects, vibrational excitons could also play a role in ion transport[31,32] in ion channels and are suggested to impact the function of ion selectivity filters,[32] where the mechanisms are still poorly understood. Additionally, quantum information protocols have previously been suggested using vibrational excitons as a medium for quantum state transfer, being stable even at room temperature,[33] dependent on the underlying relaxation and dephasing pathways. With the recent development of ultrafast real-time IR s-SNOM,[34,35] probing the formation and relaxation dynamics of vibrational excitons on the nanoscale could become accessible.

■ ASSOCIATED CONTENT

ⓢ Supporting Information

The Supporting Information is available free of charge at https://pubs.acs.org/doi/10.1021/acs.nanolett.1c01515.

Further details on sample preparations, IR s-SNOM measurements, TERS measurements, vibrational exciton modeling, tilt of 4-NTP monolayers, correlation plot between 100% 4-NTP SAM $\overline{\nu}_{s,0}^{\perp}$ and topography, 20% and 60% 4-NTP SAM spatio-spectral s-SNOM images, and average phase response of 100%, 60%, 20%, and 5% monolayers (PDF)

■ AUTHOR INFORMATION

Corresponding Author

Markus B. Raschke − *Department of Physics, Department of Chemistry, and JILA, University of Colorado, Boulder, Colorado 80309, United States;* ⓞ orcid.org/0000-0003-2822-851X; Email: markus.raschke@colorado.edu

Authors

Thomas P. Gray − *Department of Physics, Department of Chemistry, and JILA, University of Colorado, Boulder, Colorado 80309, United States;* ⓞ orcid.org/0000-0003-3422-6473

Jun Nishida − *Department of Physics, Department of Chemistry, and JILA, University of Colorado, Boulder, Colorado 80309, United States;* ⬤ orcid.org/0000-0001-7834-8179

Samuel C. Johnson − *Department of Physics, Department of Chemistry, and JILA, University of Colorado, Boulder, Colorado 80309, United States;* ⬤ orcid.org/0000-0003-0567-5026

Complete contact information is available at:
https://pubs.acs.org/10.1021/acs.nanolett.1c01515

Notes

The authors declare no competing financial interest.

■ REFERENCES

(1) Mu, X.; Gao, A.; Wang, D.; Yang, P. Self-Assembled Monolayer-Assisted Negative Lithography. *Langmuir* **2015**, *31*, 2922−2930.

(2) Casalini, S.; Bortolotti, C. A.; Leonardi, F.; Biscarini, F. Self-assembled monolayers in organic electronics. *Chem. Soc. Rev.* **2017**, *46*, 40−71.

(3) Butterworth, A.; Blues, E.; Williamson, P.; Cardona, M.; Gray, L.; Corrigan, D. K. SAM Composition and Electrode Roughness Affect Performance of a DNA Biosensor for Antibiotic Resistance. *Biosensors* **2019**, *9*, 22.

(4) Sun, J.-J.; Su, H.-S.; Yue, H.-L.; Huang, S.-C.; Huang, T.-X.; Hu, S.; Sartin, M. M.; Cheng, J.; Ren, B. Role of Adsorption Orientation in Surface Plasmon-Driven Coupling Reactions Studied by Tip-Enhanced Raman Spectroscopy. *J. Phys. Chem. Lett.* **2019**, *10*, 2306−2312.

(5) Zharnikov, M. In *Encyclopedia of Interfacial Chemistry*; Wandelt, K., Ed.; Elsevier: Oxford, U.K., 2018; pp 375−380.

(6) Jakubowicz, A.; Jia, H.; Wallace, R. M.; Gnade, B. E. Adsorption kinetics of p-nitrobenzenethiol self-assembled monolayers on a gold surface. *Langmuir* **2005**, *21*, 950−955.

(7) Sigurbjörnsson, O. F.; Firanescu, G.; Signorell, R. Vibrational exciton coupling as a probe for phase transitions and shape changes of fluoroform aerosol particles. *Phys. Chem. Chem. Phys.* **2009**, *11*, 187−194.

(8) Muller, E. A.; Gray, T. P.; Zhou, Z.; Cheng, X.; Khatib, O.; Bechtel, H. A.; Raschke, M. B. Vibrational exciton nanoimaging of phases and domains in porphyrin nanocrystals. *Proc. Natl. Acad. Sci. U. S. A.* **2020**, *117*, 7030−7037.

(9) Noh, J.; Jeong, Y.; Ito, E.; Hara, M. Formation and Domain Structure of Self-Assembled Monolayers by Adsorption of Tetrahydrothiophene on Au(111). *J. Phys. Chem. C* **2007**, *111*, 2691−2695.

(10) Nielsen, J. U.; Esplandiu, M. J.; Kolb, D. M. 4-nitrothiophenol SAM on Au(111) investigated by in situ STM, electrochemistry, and XPS. *Langmuir* **2001**, *17*, 3454−3459.

(11) Kafle, B.; Poveda, M.; Habteyes, T. G. Surface Ligand-Mediated Plasmon-Driven Photochemical Reactions. *J. Phys. Chem. Lett.* **2017**, *8*, 890−894.

(12) Zhang, Q.; Wang, H. Facet-Dependent Catalytic Activities of Au Nanoparticles Enclosed by High-Index Facets. *ACS Catal.* **2014**, *4*, 4027−4033.

(13) Vericat, C.; Vela, M. E.; Corthey, G.; Pensa, E.; Cortés, E.; Fonticelli, M. H.; Ibañez, F.; Benitez, G. E.; Carro, P.; Salvarezza, R. C. Self-assembled monolayers of thiolates on metals: a review article

on sulfur-metal chemistry and surface structures. *RSC Adv.* **2014**, *4*, 27730−27754.

(14) Dong, L.; Yang, X.; Zhang, C.; Cerjan, B.; Zhou, L.; Tseng, M. L.; Zhang, Y.; Alabastri, A.; Nordlander, P.; Halas, N. J. Nanogapped Au Antennas for Ultrasensitive Surface-Enhanced Infrared Absorption Spectroscopy. *Nano Lett.* **2017**, *17*, 5768−5774.

(15) Sun, J. J.; Su, H. S.; Yue, H. L.; Huang, S. C.; Huang, T. X.; Hu, S.; Sartin, M. M.; Cheng, J.; Ren, B. Role of Adsorption Orientation in Surface Plasmon-Driven Coupling Reactions Studied by Tip-Enhanced Raman Spectroscopy. *J. Phys. Chem. Lett.* **2019**, *10*, 2306−2312.

(16) Liou, Y.-C. M.; Yang, J.; Fasasi, A.; Griffiths, P. R. Surface-Enhanced Infrared Spectroscopic Studies of the Catalytic Behavior of Silver Nanoparticles on a Germanium Substrate. *Appl. Spectrosc.* **2011**, *65*, 528−534.

(17) You, T.; Liang, X.; Gao, Y.; Yin, P.; Guo, L.; Yang, S. A computational study on surface-enhanced Raman spectroscopy of para-substituted Benzenethiol derivatives adsorbed on gold nano-clusters. *Spectrochim. Acta, Part A* **2016**, *152*, 278−287.

(18) Nishida, J.; Alfaifi, A. H.; Gray, T. P.; Shaheen, S. E.; Raschke, M. B. Heterogeneous Cation-Lattice Interaction and Dynamics in Triple-Cation Perovskites Revealed by Infrared Vibrational Nano-scopy. *ACS Energy Letters* **2020**, *5*, 1636−1643.

(19) Muller, E. A.; Pollard, B.; Bechtel, H. A.; van Blerkom, P.; Raschke, M. B. Infrared vibrational nanocrystallography and nano-imaging. *Science Advances* **2016**, *2*, e1601006.

(20) Park, K.-D.; Raschke, M. B. Polarization Control with Plasmonic Antenna Tips: A Universal Approach to Optical Nano-crystallography and Vector-Field Imaging. *Nano Lett.* **2018**, *18*, 2912−2917.

(21) Olmon, R. L.; Rang, M.; Krenz, P. M.; Lail, B. A.; Saraf, L. V.; Boreman, G. D.; Raschke, M. B. Determination of Electric-Field, Magnetic-Field, and Electric-Current Distributions of Infrared Optical Antennas: A Near-Field Optical Vector Network Analyzer. *Phys. Rev. Lett.* **2010**, *105*, 167403.

(22) Berweger, S.; Neacsu, C. C.; Mao, Y.; Zhou, H.; Wong, S. S.; Raschke, M. B. Optical nanocrystallography with tip-enhanced phonon Raman spectroscopy. *Nat. Nanotechnol.* **2009**, *4*, 496−499.

(23) Whelan, C. M.; Smyth, M. R.; Barnes, C. J. HREELS, XPS, and electrochemical study of benzenethiol adsorption on Au(111). *Langmuir* **1999**, *15*, 116−126.

(24) Hamm, P.; Zanni, M. *Concepts and Methods of 2D Infrared Spectroscopy*; Cambridge University Press: Cambridge, U.K., 2011; pp 109−142.

(25) Hexter, R. M. Intermolecular Coupling of Vibrations in Molecular Crystals: A Vibrational Exciton Approach. *J. Chem. Phys.* **1960**, *33*, 1833−1841.

(26) Kasha, M. Energy Transfer Mechanisms and the Molecular Exciton Model for Molecular Aggregates. *Radiat. Res.* **1963**, *20*, 55−70.

(27) Goss, C. A.; Brumfield, J. C.; Irene, E. A.; Murray, R. W. Imaging and modification of gold(111) monatomic steps with atomic force microscopy. *Langmuir* **1993**, *9*, 2986−2994.

(28) Bakalis, L. D.; Rubtsov, I.; Knoester, J. Absorption spectra of mixed two-dimensional cyanine aggregates on silver halide substrates. *J. Chem. Phys.* **2002**, *117*, 5393−5403.

(29) Alberga, D.; Mangiatordi, G. F.; Motta, A.; Nicolotti, O.; Lattanzi, G. Effects of Different Self-Assembled Monolayers on Thin-Film Morphology: A Combined DFT/MD Simulation Protocol. *Langmuir* **2015**, *31*, 10693−10701.

(30) Li, X.-P.; Vanderbilt, D. Calculation of phonon-phonon interactions and two-phonon bound states on the Si(111):H surface. *Phys. Rev. Lett.* **1992**, *69*, 2543−2546.

(31) Ganim, Z.; Tokmakoff, A.; Vaziri, A. Vibrational excitons in ionophores: Experimental probes for quantum coherence-assisted ion transport and selectivity in ion channels. *New J. Phys.* **2011**, *13*, 113030.

(32) Jalalinejad, A.; Bassereh, H.; Salari, V.; Ala-Nissila, T.; Giacometti, A. Excitation energy transport with noise and disorder

in a model of the selectivity filter of an ion channel. *J. Phys.: Condens. Matter* **2018**, *30*, 415101.

(33) Pouthier, V. Vibrational exciton mediated quantum state transfer: Simple model. *Phys. Rev. B: Condens. Matter Mater. Phys.* **2012**, *85*, 214303.

(34) Dönges, S. A.; Khatib, O.; O'Callahan, B. T.; Atkin, J. M.; Park, J. H.; Cobden, D.; Raschke, M. B. Ultrafast Nanoimaging of the Photoinduced Phase Transition Dynamics in VO2. *Nano Lett.* **2016**, *16*, 3029−3035.

(35) Sternbach, A. J.; Hinton, J.; Slusar, T.; McLeod, A. S.; Liu, M. K.; Frenzel, A.; Wagner, M.; Iraheta, R.; Keilmann, F.; Leitenstorfer, A.; Fogler, M.; Kim, H.-T.; Averitt, R. D.; Basov, D. N. Artifact free time resolved near-field spectroscopy. *Opt. Express* **2017**, *25*, 28589.